

Quantum Zeno Manipulation of Quantum Dots

N. Ahmadiroz,¹ M. Geller,² J. König,² P. Kratzer,² A. Lorke,² G. Schaller,¹ and R. Schützhold^{1,3}

¹*Helmholtz-Zentrum Dresden-Rossendorf, Bautzner Landstraße 400, 01328 Dresden, Germany,*

²*Fakultät für Physik and CENIDE, Universität Duisburg-Essen, Lotharstraße 1, 47057 Duisburg, Germany,*

³*Institut für Theoretische Physik, Technische Universität Dresden, 01062 Dresden, Germany,*

(Dated: August 30, 2022)

We investigate whether and how the quantum Zeno effect, i.e., the inhibition of quantum evolution by frequent measurements, can be employed to isolate a quantum dot from its surrounding electron reservoir. In contrast to the often studied case of tunneling between discrete levels, we consider the tunnelling of an electron from a continuum reservoir to a discrete level in the dot. Realizing the quantum Zeno effect in this scenario can be much harder because the measurements should be repeated before the wave packet of the hole left behind in the reservoir moves away from the vicinity of the dot. Thus, the required repetition rate could be lowered by having a flat band (with a slow group velocity) in resonance with the dot or a sufficiently small Fermi velocity or a strong external magnetic field. We also consider the anti-Zeno effect, i.e., how measurements can accelerate or enable quantum evolution.

Introduction One of the major distinctions between classical and quantum physics is the role of measurements. As a consequence, it is impossible to directly observe quantum evolution taking place without actually affecting it. A striking example is the quantum Zeno effect which describes slowing down or even stopping quantum evolution by frequent measurements, see, e.g. [1–7].

Let us discuss the basic picture by means of a simple example, two discrete states or levels $|1\rangle$ and $|2\rangle$ of equal energy which are tunnel-coupled. Preparing the initial state in one level $|\Psi(t=0)\rangle = |1\rangle$, the time-dependent probability $P_2(t) = |\langle 2|\Psi(t)\rangle|^2$ for the other level reads $P_2(t) = \sin^2(\gamma t)$, where the frequency $\gamma > 0$ is given by the tunneling strength. For short times $t \ll 1/\gamma$, we obtain a quadratic growth $P_2(t) \approx \gamma^2 t^2$, because in quantum physics amplitudes instead of probabilities are added. However, if we measure the level occupation after such a short time, i.e., within the quadratic-growth regime, we project the state $|\Psi(t)\rangle$ back to the initial state $|1\rangle$ (assuming a strong, i.e., projective measurement) with high probability $P_1(t) \approx 1 - \gamma^2 t^2$ and thus the quantum evolution has to start again afterwards. In other words, the amplitudes before and after the measurement do no longer interfere constructively because we have obtained which-way information via the measurement. Now, repeating this measurement with a fast rate (much larger than γ) would effectively keep setting back the quantum evolution such that the quantum state stays in the initial level $|1\rangle$. This inhibition (or slowing down) of quantum evolution is usually referred to as the quantum Zeno effect [1]. Note that this line of argument crucially relies on the quadratic growth $P_2(t) \approx \gamma^2 t^2$ discussed above. In case of a linear behavior $P_2(t) \sim t$, for example, setting back the evolution by measurements would not have this retarding effect.

The quantum Zeno effect is a striking example for quantum control [8–15] and closely related to passive quantum error correction schemes (similar to the spin-

echo method). Thus, this fascinating phenomenon is of fundamental interest and has already been observed experimentally in different systems, e.g., for ions in Penning traps [2], ultra-cold atoms in optical lattices [4, 16], Bose-Einstein condensates in magnetic traps [5, 14], Rydberg atoms in cavities [6] or superconducting qubits [7].

On much shorter time scales, electrons in quantum dots are also very suitable systems for studying the quantum Zeno effect: Their energy levels and tunneling rates can be manipulated (e.g., by the variation of voltages that are applied to suitably placed gate electrodes) or the size of the dot and they have quite long coherence times while their states can be read out, i.e., measured, quite fast by capacitive charge detectors [17, 18] or optical transitions [19, 20], for example.

In most previous works, the quantum Zeno effect has been studied in a regime where the aforementioned picture based on transitions between discrete levels can be applied [2, 3, 21–25]. In the following, we shall study the more involved case of transitions between a discrete level and a continuum (a Fermi gas or liquid), see also e.g. [26, 27]. As a concrete experimental realization, we consider a quantum dot coupled to a reservoir in the form of an effectively two-dimensional electron gas (2DEG) [28–32].

The Model We consider the quantum dot-reservoir system in good approximation [33] being described by the following many-body Hamiltonian ($\hbar = 1$), cf. Fig. 1

$$\hat{H} = \int d^2r \left(\frac{(\nabla \hat{\psi}_1^\dagger) \cdot (\nabla \hat{\psi}_1)}{2m} + V_1(x, y) \hat{\psi}_1^\dagger \hat{\psi}_1 + \frac{(\nabla \hat{\psi}_2^\dagger) \cdot (\nabla \hat{\psi}_2)}{2m} + (\gamma \hat{\psi}_1^\dagger \hat{\psi}_2 + \text{h.c.}) \right). \quad (1)$$

The first line represents the quantum dot for which we employ the standard [34] harmonic potential approximation $V_1(x, y) = V_0 + m\omega^2(x^2 + y^2)/2$ where the offset V_0 can be tuned by a gate voltage. The second line de-

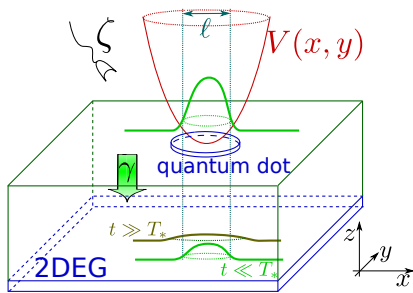


FIG. 1. Sketch of the quantum dot with confinement potential $V(x, y)$ coupled to the effectively two-dimensional electron gas (2DEG), both realized as lowest quantum well states. Tunneling with strength γ of an electron or hole wave-packet with characteristic size ℓ from the dot to the 2DEG reservoir corresponds to discharging or charging. In the reservoir, the wave-packets then spread or move away on a typical time scale T_* which limits the repetition rate of the measurement (indicated by ζ) required for observing the quantum Zeno effect.

scribes the reservoir and its tunnel coupling to the dot with the coupling strength γ . The field operators $\hat{\psi}_1(x, y)$ and $\hat{\psi}_2(x, y)$ could be envisaged as lowest quantum well states in z -direction, for example, where we assume that the energies of the higher quantum well states are so large (tight confinement limit) that we can neglect them.

If we focus on the ground state of the quantum dot $\hat{\psi}_1(x, y) \rightarrow \Phi_0(x, y)\hat{a}_d$ and Fourier transform the reservoir modes $\hat{\psi}_2(x, y) \rightarrow \hat{\psi}_{\mathbf{k}}$, the Hamiltonian (1) becomes

$$\hat{H} = \epsilon_d \hat{n}_d + \int d^2k \left[\epsilon_{\mathbf{k}} \hat{\psi}_{\mathbf{k}}^\dagger \hat{\psi}_{\mathbf{k}} + \left(\gamma_{\mathbf{k}} \hat{a}_d^\dagger \hat{\psi}_{\mathbf{k}} + \text{h.c.} \right) \right], \quad (2)$$

where ϵ_d denotes the energy of the quantum dot level and $\hat{n}_d = \hat{a}_d^\dagger \hat{a}_d$ the corresponding number operator, while $\epsilon_{\mathbf{k}} = \mathbf{k}^2/(2m)$ are the single-particle energies of the reservoir modes $\mathbf{k} = (k_x, k_y)$. Finally, $\gamma_{\mathbf{k}}$ is determined by the Fourier transform of the ground-state wave-function inside the quantum dot (see e.g. [35]), i.e., Gaussian

$$\gamma_{\mathbf{k}} = \gamma \int \frac{d^2r}{2\pi} \Phi_0^*(x, y) e^{+i\mathbf{k}\cdot\mathbf{r}} = \gamma_0 \exp \left\{ -\frac{1}{2} \mathbf{k}^2 \ell^2 \right\}, \quad (3)$$

where $\ell = \sqrt{\hbar/(m\omega)}$ is the characteristic dot length scale. Note that the bi-linear Hamiltonian (1) does not explicitly include non-linear (e.g., Coulomb) interactions between the electrons nor their coupling to other degrees of freedom (e.g., phonons) whose potential impact will be discussed below. Therefore, we restrict ourselves to studying the transition between an empty and a singly-occupied dot, for which a charging energy of the quantum dot is irrelevant.

Quantum Zeno Dynamics Now we are in the position to study the tunneling process of an electron from the reservoir into the quantum dot. We start with the initial state $|\text{in}\rangle$ where the dot is empty $\hat{a}_d |\text{in}\rangle = 0$ while the reservoir is filled up to the Fermi energy.

Although the above model can be solved exactly using, e.g., Greens function techniques [36], we may already calculate the time-dependent probability $P(t)$ for the occupation of the quantum dot using standard time-dependent perturbation theory with respect to γ ,

$$P(t) = \langle \hat{n}_d(t) \rangle = 4 \int_{\text{F}} d^2k |\gamma_{\mathbf{k}}|^2 \frac{\sin^2([\epsilon_d - \epsilon_{\mathbf{k}}]t/2)}{(\epsilon_d - \epsilon_{\mathbf{k}})^2}, \quad (4)$$

where the subscript F on the integral indicates that the integration runs up to Fermi energy ϵ_{F} .

Quantum-Zeno Regime Even within the region of applicability of perturbation theory (i.e., for small probabilities $P(t) \ll 1$), we obtain two temporal regimes. For small times t , the probability $P(t)$ grows quadratically

$$P(t) = t^2 \int_{\text{F}} d^2k |\gamma_{\mathbf{k}}|^2 + \mathcal{O}(t^3). \quad (5)$$

For the Gaussian case (3), this simplifies to

$$P(t) = \pi \frac{\gamma_0^2 t^2}{\ell^2} (1 - \exp\{-k_{\text{F}}^2 \ell^2\}) + \mathcal{O}(t^3), \quad (6)$$

where $k_{\text{F}} = \sqrt{2m\epsilon_{\text{F}}}$ denotes the Fermi momentum. If the Fermi energy ϵ_{F} is large enough $2m\epsilon_{\text{F}}\ell^2 \gg 1$, i.e., $k_{\text{F}}^2\ell^2 \gg 1$, we obtain $P(t) = \pi\gamma_0^2 t^2/\ell^2$. In the opposite limit $k_{\text{F}}^2\ell^2 \ll 1$, the integration is cut off by k_{F}^2 and we find $P(t) = \pi\gamma_0^2 t^2 k_{\text{F}}^2$.

Regime of Fermi's Golden Rule For later times (but still in the perturbative regime $P(t) \ll 1$), we can use the standard approximation of the sinc function in Eq. (4) by a Dirac delta function and obtain a linear growth in time, consistent with Fermi's Golden Rule

$$P(t) \approx 2\pi t \int_{\text{F}} d^2k |\gamma_{\mathbf{k}}|^2 \delta(\epsilon_d - \epsilon_{\mathbf{k}}). \quad (7)$$

Obviously, the above integral vanishes for $\epsilon_d > \epsilon_{\text{F}}$ and for $\epsilon_d < 0$, i.e., if there are no filled reservoir modes in resonance with the dot. (These cases are discussed in the supplement.) Assuming $\epsilon_{\text{F}} > \epsilon_d > 0$, we find for the Gaussian case (3) with $\epsilon_{\mathbf{k}} = \mathbf{k}^2/(2m)$

$$P(t) \approx (2\pi)^2 t m \gamma_0^2 \exp\{-2m\epsilon_d \ell^2\}. \quad (8)$$

The exponential suppression $\exp\{-2m\epsilon_d \ell^2\}$ for large dot energies $2m\epsilon_d \ell^2 \gg 1$ stems from the wave-function mismatch between the Gaussian ground-state wave-function of the dot and the reservoir wave-functions of the corresponding energy ϵ_d which are rapidly oscillating for large ϵ_d . In order to avoid this suppression, we assume small dot energies $2m\epsilon_d \ell^2 \ll 1$ in the following.

As a peculiarity of the case of two spatial dimensions, the remaining pre-factor $P(t) \approx (2\pi)^2 t m \gamma_0^2$ is actually independent of ϵ_d because the energy $\epsilon_{\mathbf{k}} = \mathbf{k}^2/(2m)$ and the volume factor d^2k both display the same quadratic scaling in k , such that the density of states per energy is constant.

Crossover Time Having found an initial period of quadratic growth (5) for early times (quantum Zeno regime) followed by a period of linear growth (7) for later times (regime of Fermi's Golden Rule), we may estimate the crossover time T_* marking the transition between the two regimes [37] by comparing Eqs. (5) and (7). For the Gaussian limit we obtain with (6) and (8)

$$T_* \approx 4\pi m \ell^2 \frac{\exp\{-2m\epsilon_d \ell^2\}}{1 - \exp\{-\ell^2 k_F^2\}}. \quad (9)$$

Assuming small dot excitation energies $2m\epsilon_d \ell^2 \ll 1$ and considering the limiting cases as discussed after Eq. (6), this simplifies to $T_* \approx 4\pi m \ell^2$ for $\ell^2 k_F^2 \gg 1$ and to $T_* \approx 4\pi m/k_F^2$ for $\ell^2 k_F^2 \ll 1$, respectively.

As explained in the Introduction, only measurements with a repetition time faster than T_* can induce the quantum Zeno effect. This time scale is typically quite short and can be visualized by the following intuitive picture.

Let us first consider the case $\ell^2 k_F^2 \gg 1$. If an electron tunnels with a small amplitude from the reservoir to the quantum dot, it leaves behind a hole in the reservoir. The typical size of the initial wave packet of this hole is determined by the characteristic length ℓ of the ground-state wave function of the dot. Afterwards, this wave packet is spreading out or moving away with the typical group velocity at that length scale $v_{\text{group}} \propto 1/(\ell m)$. Once the wave packet has spread out too much or moved away too far, further tunneling amplitudes would not be added coherently and probabilities would add up instead. This is precisely the transition from the quantum Zeno regime to the regime of Fermi's Golden Rule occurring at the crossover time $T_* \sim \ell/v_{\text{group}}$.

In the opposite limit ($k_F^2 \ell^2 \ll 1$), one should just replace the length scale ℓ of the dot by the Fermi length $\ell_F \propto 1/k_F$ and the associated group velocity by the Fermi velocity $v_F = k_F/m$. Then, the crossover time T_* is basically the Fermi time T_F which is related to the Fermi energy ϵ_F by Heisenberg's uncertainty relation [$T_* = \mathcal{O}\{\epsilon_F^{-1}\}$] and determines the minimum response time of hole states in the reservoir.

Consistent with the results of [38], an effectively Markovian reservoir is obtained in the combined limit of $\ell \rightarrow 0$ and $k_F \rightarrow \infty$ where the available density of states in the reservoir becomes constant and the quantum-Zeno regime/effect disappears $T_* = 0$.

General Band Structure Let us now discuss possible generalizations of the above results (see also the supplement). For reservoir electrons propagating in a lattice, the single-particle energies $\epsilon_{\mathbf{k}}$ of the reservoir modes \mathbf{k} should be replaced by the lattice band structure, which might also modify the (experimentally accessible [39]) couplings $\gamma_{\mathbf{k}}$ accordingly. Of course, the same would happen for non-harmonic quantum dot potentials $V_1(x, y) \neq V_0 + m\omega^2(x^2 + y^2)/2$. Nevertheless, one would still expect the effective Hamiltonian (2) to provide a good approximation. Thus, the results (4) and

thus (5) and (7) remain valid, but with modified $\epsilon_{\mathbf{k}}$ and $\gamma_{\mathbf{k}}$. This may entail interesting consequences. For example, if we have a flat band (with $\epsilon_{\mathbf{k}} = \text{const}$) below the Fermi energy in resonance with the quantum dot (i.e., $\epsilon_{\mathbf{k}} = \text{const} = \epsilon_d$), the probability (7) per time would become very large while the initial growth (5) would remain almost unaffected since it is independent of $\epsilon_{\mathbf{k}}$. This means that the crossover time T_* would also become very large, which might help observing the quantum Zeno effect in this scenario. In terms of the intuitive picture sketched above, the group velocity becomes very small for such a flat band such that the wave packet stays quite long in the vicinity of the dot.

Magnetic Field The above finding regarding flat or nearly flat bands motivates the study of a strong external magnetic field perpendicular to the reservoir, because this does also turn the reservoir modes into flat bands in the form the well-known Landau levels.

As usual, we represent the constant perpendicular magnetic field $\mathbf{B} = B\mathbf{e}_z$ in the symmetric gauge by the vector potential $\mathbf{A} = \mathbf{B} \times \mathbf{r}/2$. Then, after minimal coupling $\nabla \rightarrow \nabla - q\mathbf{A}$ to the electron charge q , the Hamiltonian (1) acquires an additional angular-momentum contribution $-2\mathbf{A} \cdot \nabla = \mathbf{B} \cdot \hat{\mathbf{L}} = B\hat{L}_z$ as well as a harmonic confinement potential $V_B = \Omega_B^2(x^2 + y^2)/8$ from the quadratic term $\mathbf{A}^2 = B^2(x^2 + y^2)/4$ where Ω_B is the cyclotron frequency $\Omega_B = qB/m$.

Thus, the reservoir eigen-functions are no longer plane waves as in Eq. (2), but discrete Landau levels which can be represented by the modes of a two-dimensional harmonic oscillator in polar coordinates r and φ [40]

$$\psi_{n,l}(r, \varphi) = f_{n,l}(r)e^{il\varphi}. \quad (10)$$

Here $n \in \mathbb{N}$ and $l \in \mathbb{Z}$ are the quantum numbers corresponding to energy $\epsilon_n = \Omega_B(n + 1/2)$ and angular momentum \hat{L}_z , respectively. The radial mode functions $f_{n,l}(r)$ are given by polynomials multiplied by a Gaussian $\exp\{-r^2/(2\ell_B)^2\}$ with the magnetic length $\ell_B = 1/\sqrt{qB}$. For example, the lowest Landau levels with $n = 0$ have $f_{n=0,l}(r) \propto r^l \exp\{-r^2/(2\ell_B)^2\}$ with $l \geq 0$, which can be experimentally mapped [30, 41].

The ground-state wave function of the quantum dot will also be modified, but merely by the additional harmonic confinement potential $V_B = \Omega_B^2(x^2 + y^2)/8$ which narrows the Gaussian wave-function (i.e., decreases ℓ) and increases the energy ϵ_d . Since this wave function is rotationally symmetric (i.e., has zero angular momentum), it only tunnel couples to reservoir modes with $l = 0$.

If we now assume a strong magnetic field B and/or a small Fermi energy $\epsilon_F < 3\Omega_B/2$ such that only the lowest Landau levels are occupied, the effective Hamiltonian (2) can be restricted to the mode $n = l = 0$ and reads

$$\hat{H} = \epsilon_d \hat{n}_d + \frac{\Omega_B}{2} \hat{n}_{0,0} + \left(\gamma_{0,0} \hat{a}_d^\dagger \hat{a}_{0,0} + \text{h.c.} \right), \quad (11)$$

where the effective tunnel coupling $\gamma_{0,0}$ is determined by the overlap of the two Gaussian wave functions of the dot and $\psi_{0,0} \propto \exp\{-r^2/(2\ell_B)^2\}$.

Assuming resonance $\epsilon_d = \Omega_B/2$, this Hamiltonian (11) is then formally equivalent to tunneling between two discrete modes (described by \hat{a}_d and $\hat{a}_{0,0}$) such that we are back to the original picture of the quantum Zeno effect as described in the Introduction. Off-resonant scenarios $\epsilon_d \neq \Omega_B/2$ may give rise to the anti-Zeno effect [4, 8, 23, 42], as discussed in the supplement.

Measurement Model So far, the Hamiltonian (1) does only describe the internal dynamics of the electrons, but not the actual measurement process – which is causing the quantum Zeno effect. To incorporate this, let us construct a simple toy model for the read out. We assume that the dot is strongly illuminated by laser light (saturation regime) which quickly transfers the electron in the quantum dot from the ground state level to an excited level $\hat{a}_d \hat{a}_e^\dagger$ as soon as the dot is occupied. This excited level then rapidly decays by emitting a photon as described by the bosonic creation and annihilation operators \hat{b}^\dagger and \hat{b} , where we focus on one mode for simplicity. Assuming that these excitation–de-excitation cycles occur much faster than all the other time scales considered above (e.g., T_*), we may use an effective description where the dot emits photons as soon as it is occupied. Thus, we model the measurement by the additional Hamiltonian

$$\hat{H}_{\text{measure}} = \hat{n}_d \left(i\zeta \hat{b}^\dagger + \text{h.c.} \right) \quad (12)$$

with the detector coupling strength $\zeta > 0$, which is basically a pointer Hamiltonian for measuring the observable \hat{n}_d .

Since \hat{H}_{measure} commutes with the undisturbed Hamiltonian $\hat{H}_0 = \epsilon_d \hat{n}_d + \int d^2k \epsilon_{\mathbf{k}} \hat{\psi}_{\mathbf{k}}^\dagger \hat{\psi}_{\mathbf{k}}$, we may incorporate it easily into the time-dependent perturbation theory used above for calculating $P(t)$. In the interaction picture, the dot annihilation operator \hat{a}_d just acquires an additional operator-valued factor

$$\hat{a}_d(t) = e^{-i\epsilon_d t} \exp \left\{ (\zeta \hat{b}^\dagger - \text{h.c.}) t \right\} \hat{a}_d(0), \quad (13)$$

which represents the dynamics induced by $\hat{H}_0 + \hat{H}_{\text{measure}}$. When acting on the initial photonic vacuum state $|0\rangle$ with $\hat{b}|0\rangle = 0$, this additional factor $\exp\{(\zeta \hat{b}^\dagger - \text{h.c.})t\}$ just generates a coherent state $|\alpha(t)\rangle$ of the photon field whose amplitude $\alpha(t) = \zeta t$ grows linearly with time t .

The overlap of these coherent states at different times $\langle \alpha(t_1) | \alpha(t_2) \rangle = e^{-\zeta^2(t_1 - t_2)^2/2}$ modifies Eq. (4) via

$$P(t) = \int_0^t dt_1 \int_0^t dt_2 \int_{\mathbb{F}} d^2k |\gamma_{\mathbf{k}}|^2 \exp \left\{ -\frac{\zeta^2}{2} (t_1 - t_2)^2 \right\} \times \exp \left\{ -i(\epsilon_d - \epsilon_{\mathbf{k}})(t_1 - t_2) \right\}. \quad (14)$$

For very short times $t \ll T_*$ and $t \ll 1/\zeta$, we recover the initial quadratic growth in Eq. (5). What happens

after that initial period depends on the quantity ζT_* . For small $\zeta T_* \ll 1$, we recover Eq. (7). For large $\zeta T_* \gg 1$, on the other hand, the probability is strongly suppressed

$$P(t) \sim t \frac{\sqrt{2}}{\zeta} \int_{\mathbb{F}} d^2k |\gamma_{\mathbf{k}}|^2, \quad (15)$$

which is a manifestation of the quantum Zeno effect by frequent measurements with the effective rate ζ .

The detector signal can be very explicitly evaluated with methods of Full Counting Statistics or quantum polyspectra [24, 43]. However, already the analysis of average values reveals (see supplement) that – although delay effects occur – a transition between the timescales can be directly resolved.

Conclusions For the example of a quantum dot tunnel coupled to an effectively two-dimensional electron reservoir, we study whether and how the quantum Zeno effect can be employed to suppress tunneling between a discrete level and a continuum. In contrast to tunneling between two discrete levels, we find that the required measurement repetition rate is set by the time T_* it takes the wave-packet in the reservoir to move away from the vicinity of the quantum dot. Hence this time scale can be increased (and thus the required repetition rate decreased) by lowering the Fermi energy or having a flat band (thus reducing the Fermi velocity) or by applying a strong perpendicular magnetic field, which effectively localizes the reservoir modes.

In a bigger picture, suppressing tunneling via the quantum Zeno effect and thereby effectively isolating the quantum dot from its environment is quite analogous to passive quantum error correcting schemes, such as the spin echo method. In contrast to active quantum error correcting schemes (typically involving redundancies), such passive schemes are based on interrupting the coherence between the quantum dot or qubit and its environment such that the constructive interference of the error amplitudes is turned into a (at least partially) destructive interference. As an intuitive picture, these methods work well as long as the wave-packet associated with the quantum error is still “lurking” in the vicinity of the quantum dot or qubit. Once they moved too far away, the impact of measurements or echo sequences is strongly reduced.

As an outlook, frequent measurements can also enable or accelerate quantum evolution, which is usually referred to as the anti-Zeno effect [42]. As shown in the supplement, this effect can in principle also be realized in quantum dots, opening further windows for manipulation.

Experimental scenarios In order to discuss the experimental relevance of our findings, let us insert typical experimental parameters. For an effective mass of around 7 % of the electron mass [44] and a 2D electron density between 3 and $6 \times 10^{11} \text{ cm}^{-2}$, we get Fermi energies between 10 and 20 meV and Fermi velocities between

2 and 4×10^5 m/s. Assuming a typical level spacing in the quantum dot of around 50 meV [34, 44], the characteristic length scale of the ground state wave function is $\ell \approx 5$ nm. With a Fermi momentum of order 10^8 m $^{-1}$, we have $k_F \ell$ of order unity. Thus, we may estimate the crossover time T_* by comparing the Fermi velocity with the length scale $\ell \approx 5$ nm which yields rather short times of order $T_* = \mathcal{O}(10$ fs). Unfortunately, although measurements can be performed quite fast (on the nano-second scale [20]), this $T_* = \mathcal{O}(10$ fs) is probably too short to observe the quantum Zeno effect in this set-up. Increasing this time scale T_* by decreasing the Fermi energy (i.e., reducing the electron density in the reservoir) or by using materials with a flat band is possible in principle, but experimentally quite challenging.

Thus, probably the most viable option is to apply a strong perpendicular magnetic field B , say, of around 10 T, such that the 2DEG is in the Quantum Hall regime [45]. The resulting magnetic length of $\ell_B \approx 8$ nm is roughly of the same order as the length scale $\ell \approx 5$ nm associated with the quantum dot and similarly the Landau level spacing of about 15 meV is not too far away from the other energy scales. With aligning the energy levels accordingly, one can arrange resonant tunnel transitions between the discrete level of the quantum dot and one of the discrete Landau levels in the reservoir. In this case, the line of arguments sketched in the Introduction can be applied and thus the measurement repetition rate is set by the tunneling rate γ between these two levels. Since the time associated scale $1/\gamma$ can be quite long (in the micro- to milli-second regime or even longer, which would also enable an electric readout [17, 18]), a measurement time in the nano-second regime should be sufficient to observe the quantum Zeno effect.

In order to enable such an observation, one has to make sure that the environmental decoherence (which can have basically the same effect as a measurement; for a review of tunneling in a dissipative environment see e.g. [46]) is weak enough, i.e., the associated coherence time is longer than the time between measurements. A frequently discussed decoherence mechanism is the scattering of the electrons or holes in the reservoir at local impurities. As long as these impurities (which can be characterized experimentally [47]) are not too dense and thus far away from the dot, this mechanism is not relevant here because, as explained above, if the reservoir wave packet moved away from the dot far enough to see the impurity, it is already outside the region of applicability of the quantum Zeno effect. Another potentially important mechanism stems from the Coulomb interaction between the electrons or holes or their interaction with phonons. In order to suppress this decoherence mechanism, the temperature should be low enough such that the available phase space and number of excitations is reduced.

Also in this respect, working in a strong magnetic field can be helpful: While electron-phonon scatter-

ing in a field-free 2DEG happens in two-dimensional k -space, in the Quantum Hall regime electron-phonon scattering is limited to the one-dimensional (both in real-space and k -space) lines along which the electrons drifts. This reduced dimensionality strongly suppresses electron-phonon scattering and renders it negligible at milli-Kelvin temperatures. At these temperatures T , electron-electron scattering is the only relevant mechanism and follows a T^2 law [48] in a 2DEG in a strong magnetic field. Experimental studies of the universality in the Quantum Hall regime [49] allow one to estimate the associated time scale.

R.S. acknowledges valuable discussions with S. Popescu and W.G. Unruh. Funded by the Deutsche Forschungsgemeinschaft (DFG, German Research Foundation) – Project-ID 278162697 – SFB 1242.

-
- [1] B. Misra and E. C. G. Sudarshan. The Zeno's paradox in quantum theory. *Journal of Mathematical Physics*, 18:756, 1977.
 - [2] W. M. Itano, D. J. Heinzen, J. J. Bollinger, and D. J. Wineland. Quantum Zeno effect. *Phys. Rev. A*, 41:2295–2300, Mar 1990.
 - [3] G. Hackenbroich, B. Rosenow, and H. A. Weidenmüller. Quantum Zeno effect and parametric resonance in mesoscopic physics. *Phys. Rev. Lett.*, 81:5896–5899, Dec 1998.
 - [4] M. C. Fischer, B. Gutiérrez-Medina, and M. G. Raizen. Observation of the quantum Zeno and anti-Zeno effects in an unstable system. *Phys. Rev. Lett.*, 87:040402, Jul 2001.
 - [5] E. W. Streed, J. Mun, M. Boyd, G. K. Campbell, P. Medley, W. Ketterle, and D. E. Pritchard. Continuous and pulsed quantum Zeno effect. *Phys. Rev. Lett.*, 97:260402, Dec 2006.
 - [6] J. Bernu, S. Deléglise, C. Sayrin, S. Kuhr, I. Dotsenko, M. Brune, J. M. Raimond, and S. Haroche. Freezing coherent field growth in a cavity by the quantum Zeno effect. *Phys. Rev. Lett.*, 101:180402, Oct 2008.
 - [7] D. H. Slichter, C. Müller, R. Vijay, S. J. Weber, A. Blais, and I. Siddiqi. Quantum Zeno effect in the strong measurement regime of circuit quantum electrodynamics. *New Journal of Physics*, 18(5):053031, may 2016.
 - [8] P. Facchi, H. Nakazato, and S. Pascazio. From the quantum Zeno to the inverse quantum Zeno effect. *Phys. Rev. Lett.*, 86:2699–2703, Mar 2001.
 - [9] P. Facchi and S. Pascazio. Quantum Zeno subspaces. *Physical Review Letters*, 89:080401, 2002.
 - [10] P. Facchi, D. A. Lidar, and S. Pascazio. Unification of dynamical decoupling and the quantum Zeno effect. *Physical Review A*, 69:032314, 2004.
 - [11] H. M. Wiseman and G. J. Milburn. *Quantum Measurement and Control*. Cambridge University Press, Cambridge, 2010.
 - [12] G. A. Álvarez, D. D. B. Rao, L. Frydman, and G. Kurizki. Zeno and anti-zeno polarization control of spin ensembles by induced dephasing. *Phys. Rev. Lett.*, 105:160401, Oct 2010.
 - [13] G. A. Paz-Silva, A. T. Rezakhani, J. M. Dominy, and

- D. A. Lidar. Zeno effect for quantum computation and control. *Physical Review Letters*, 108:080501, 2012.
- [14] F. Schäfer, I. Herrera, S. Cherukattil, C. Lovecchio, F. Cataliotti, F. Caruso, and A. Smerzi. Experimental realization of quantum Zeno dynamics. *Nature Communications*, 5:3194, 2014.
- [15] G. Barontini, L. Hohmann, F. Haas, J. Estève, and J. Reichel. Deterministic generation of multiparticle entanglement by quantum zeno dynamics. *Science*, 349(6254):1317–1321, 2015.
- [16] B. Zhu, B. Gadway, M. Foss-Feig, J. Schachenmayer, M. L. Wall, K. R. A. Hazzard, B. Yan, S. A. Moses, J. P. Covey, D. S. Jin, J. Ye, M. Holland, and A. M. Rey. Suppressing the loss of ultracold molecules via the continuous quantum Zeno effect. *Phys. Rev. Lett.*, 112:070404, Feb 2014.
- [17] T. Fujisawa, T. Hayashi, R. Tomita, and Y. Hirayama. Bidirectional counting of single electrons. *Science*, 312:1634–1636, 2006.
- [18] C. Flindt, C. Fricke, F. Hohls, T. Novotny, K. Netocny, T. Brandes, and R. J. Haug. Universal oscillations in counting statistics. *PNAS*, 106:10116–10119, 2009.
- [19] A. Kurzmann, B. Merkel, P. A. Labud, A. Ludwig, A. D. Wieck, A. Lorke, and M. Geller. Optical blocking of electron tunneling into a single self-assembled quantum dot. *Phys. Rev. Lett.*, 117:017401, Jun 2016.
- [20] A. Kurzmann, P. Stegmann, J. Kerski, R. Schott, A. Ludwig, A. D. Wieck, J. König, A. Lorke, and M. Geller. Optical detection of single-electron tunneling into a semiconductor quantum dot. *Phys. Rev. Lett.*, 122:247403, Jun 2019.
- [21] S. A. Gurvitz, L. Fedichkin, D. Mozysky, and G. P. Berman. Relaxation and the Zeno effect in qubit measurements. *Phys. Rev. Lett.*, 91:066801, Aug 2003.
- [22] S. A. Gurvitz. Quantum limit of measurement and the projection postulate. *International Journal of Modern Physics B*, 20:1363, 2006.
- [23] D. Segal and D. R. Reichman. Zeno and anti-Zeno effects in spin-bath models. *Phys. Rev. A*, 76:012109, Jul 2007.
- [24] G. Schaller, J. Cerrillo, G. Engelhardt, and P. Strasberg. Electronic Maxwell demon in the coherent strong-coupling regime. *Phys. Rev. B*, 97:195104, May 2018.
- [25] N. V. Leppen and D. S. Smirnov. Optical measurement of electron spins in quantum dots: Quantum zeno effects. *arXiv*, page arXiv:2202.13994, 2022.
- [26] S. A. Gurvitz. Measurements with a noninvasive detector and dephasing mechanism. *Phys. Rev. B*, 56:15215–15223, Dec 1997.
- [27] G. Engelhardt and G. Schaller. Maxwell’s demon in the quantum-Zeno regime and beyond. *New Journal of Physics*, 20:023011, 2018.
- [28] T. Ando, A. B. Fowler, and F. Stern. Electronic properties of two-dimensional systems. *Rev. Mod. Phys.*, 54:437–672, Apr 1982.
- [29] S. M. Reimann and M. Manninen. Electronic structure of quantum dots. *Rev. Mod. Phys.*, 74:1283–1342, Nov 2002.
- [30] M. Russ, A. Lorke, D. Reuter, and P. Schafmeister. Self-assembled quantum dots as probes for Landau-level spectroscopy. *Physica E: Low-dimensional Systems and Nanostructures*, 22(1):506–509, 2004. 15th International Conference on Electronic Properties of Two-Dimensional Systems (EP2DS-15).
- [31] M. Ruß, C. Meier, A. Lorke, D. Reuter, and A. D. Wieck. Role of quantum capacitance in coupled low-dimensional electron systems. *Phys. Rev. B*, 73:115334, Mar 2006.
- [32] M. Geller. Nonequilibrium carrier dynamics in self-assembled quantum dots. *Applied Physics Reviews*, 6(3):031306, 2019.
- [33] E. E. Vdovin, A. Levin, A. Patanè, L. Eaves, P. C. Main, Y. N. Khanin, Y. V. Dubrovskii, M. Henini, and G. Hill. Imaging the electron wave function in self-assembled quantum dots. *Science*, 290(5489):122–124, 2000.
- [34] R. J. Warburton, B. T. Miller, C. S. Dürr, C. Bödefeld, K. Karrai, J. P. Kotthaus, G. Medeiros-Ribeiro, P. M. Petroff, and S. Huan. Coulomb interactions in small charge-tunable quantum dots: A simple model. *Phys. Rev. B*, 58:16221–16231, Dec 1998.
- [35] O. S. Wibbelhoff, A. Lorke, D. Reuter, and A. D. Wieck. Magnetocapacitance probing of the many-particle states in inas dots. *Applied Physics Letters*, 86(9):092104, 2005.
- [36] H. Haug and A.-P. Jauho. *Quantum Kinetics in Transport and Optics of Semiconductors*. Springer, Berlin, 2008.
- [37] R. Schützhold and G. Gnanapragasam. Quantum Zeno suppression of three-body losses in Bose-Einstein condensates. *Physical Review A*, 82:022120, 2010.
- [38] S. A. Gurvitz. Josephson-type effect in resonant-tunneling heterostructures. *Physical Review B*, 44:11924–11932, 1991.
- [39] D. Zhou, A. Beckel, A. Ludwig, A. D. Wieck, M. Geller, and A. Lorke. Tuning the tunneling probability between low-dimensional electron systems by momentum matching. *Applied Physics Letters*, 106(24):243105, 2015.
- [40] O. Ciftja. Detailed solution of the problem of Landau states in a symmetric gauge. *European Journal of Physics*, 41(3):035404, apr 2020.
- [41] W. Lei, C. Notthoff, J. Peng, D. Reuter, A. Wieck, G. Bester, and A. Lorke. “artificial atoms” in magnetic fields: Wave-function shaping and phase-sensitive tunneling. *Phys. Rev. Lett.*, 105:176804, Oct 2010.
- [42] A. G. Kofman and G. Kurizki. Acceleration of quantum decay processes by frequent observations. *Nature*, 405:546, 2000.
- [43] M. Sift, A. Kurzmann, J. Kerski, R. Schott, A. Ludwig, A. D. Wieck, A. Lorke, M. Geller, and D. Hägele. Quantum polyspectra for modeling and evaluating quantum transport measurements: A unifying approach to the strong and weak measurement regime. *Phys. Rev. Research*, 3:033123, Aug 2021.
- [44] M. Fricke, A. Lorke, J. P. Kotthaus, G. Medeiros-Ribeiro, and P. M. Petroff. Shell structure and electron-electron interaction in self-assembled InAs quantum dots. *Europhysics Letters (EPL)*, 36(3):197–202, oct 1996.
- [45] In the Quantum Hall regime, small residual electric fields within the 2DEG that originate e.g. from interface roughness or electrostatic potential fluctuations introduced by the QDs will result in a drift of the wave packet in crossed \mathbf{E} and \mathbf{B} fields. The drift velocity $\mathbf{v}_{\text{drift}} = c(\mathbf{E} \times \mathbf{B})$ is, however, much lower than the Fermi velocity in the original, field-free 2DEG. Thus, the problem of a temporally decreasing overlap is diminished.
- [46] A. Caldeira and A. Leggett. Quantum tunnelling in a dissipative system. *Annals of Physics (N. Y.)*, 149:374, 1983.
- [47] J. Kerski, P. Lochner, A. Ludwig, A. Wieck, A. Kurzmann, A. Lorke, and M. Geller. Quantum sensor for

nanoscale defect characterization. *Phys. Rev. Applied*, 15:024029, Feb 2021.

- [48] B. L. Altshuler, A. B. Aronov, and D. E. Khmelnitsky. Effects of electron-electron collisions with small energy transfers on quantum localisation. *J. Phys. C*, 15:7367, 1982.
- [49] S. Koch, R. J. Haug, K. von Klitzing, and K. Ploog. Direct measurement of critical exponents in the quantum Hall regime. *Surf. Sci.*, 263:108 – 111, 1992.
- [50] A. Nazir and G. Schaller. The reaction coordinate mapping in quantum thermodynamics. In F. Binder, L. A. Correa, C. Gogolin, J. Anders, and G. Adesso, editors, *Thermodynamics in the quantum regime – Recent progress and outlook*, Fundamental Theories of Physics, page 551. Springer, Cham, 2019.
- [51] N. Martensen and G. Schaller. Transmission from reverse reaction coordinate mappings. *European Physical Journal B*, 92:30, 2019.
- [52] G. T. Landi, D. Poletti, and G. Schaller. Non-equilibrium boundary driven quantum systems: models, methods and properties. *Reviews of Modern Physics (in press)*, page arXiv:2104.14350, 2022.

Detector dynamics

To evaluate the detector occupation, we first note that in the interaction picture, the photon annihilation operator grows linearly in time

$$\hat{b}(t) = \hat{b}(0) + \zeta t \hat{n}_d(0). \quad (16)$$

The actually emitted photon number of our toy model then becomes to second order perturbation theory

$$\langle \hat{b}^\dagger \hat{b} \rangle_t = \zeta^2 \int_0^t dt_1 \int_0^t dt_2 \int_{\text{F}} d^2k |\gamma_{\mathbf{k}}|^2 \exp \left\{ -\frac{\zeta^2}{2} (t_1 - t_2)^2 \right\} \times (t - t_1)(t - t_2) \exp \{ -i(\epsilon_d - \epsilon_{\mathbf{k}})(t_1 - t_2) \}, \quad (17)$$

which also reflects the crossover from a t^4 scaling for $t \ll T_*$ and $t\zeta \ll 1$ to a reduced – at most t^3 – scaling for $t \gg T_*$. The initial delayed response can be understood as the detector has to react to the dynamics of the system first. If the detector is used to reveal the Zeno suppression as a primary system, one should keep in mind that the detector delay also imposes a lower bound on the measurement time. For example, when the dot is initially filled, already the lowest order contributes and we would obtain $\langle \hat{b}^\dagger \hat{b} \rangle_t \approx \zeta^2 t^2$. Thus, if N_{thr} denotes the minimum number of photons allowing to discriminate a charged dot from an empty dot, we obtain a lower bound on the measurement time $\zeta t \geq \sqrt{N_{\text{thr}}}$. To investigate whether one can simultaneously realize a Zeno-freezing of the dot while faithfully detecting it with the same primary detector, we can analytically perform the temporal integrals in Eq. (14). A quadratic temporal scaling is still possible but then puts tighter constraints on the γ_k .

The expectation value of a photon annihilation operator (relevant e.g. for homodyne measurements) would

become instead

$$\langle \hat{b} \rangle_t = \zeta \int_0^t dt_1 \int_0^t dt_2 \int_{\text{F}} d^2k |\gamma_{\mathbf{k}}|^2 \exp \left\{ -\frac{\zeta^2}{2} (t_1 - t_2)^2 \right\} \times (t - t_2) \exp \{ -i(\epsilon_d - \epsilon_{\mathbf{k}})(t_1 - t_2) \} \quad (18)$$

and exhibits a crossover from a cubic to (at most) quadratic scaling.

Considering the effect of a finite detector frequency $\hat{H}_{\text{measure}} \rightarrow \hat{H}_{\text{measure}} + \omega_{\text{det}} \hat{b}^\dagger \hat{b}$ implies an oscillatory behaviour of $\hat{b}(t)$ in the interaction picture and would eventually again lead to a linear long-term scaling in the Fermi golden rule regime.

Measuring empty dots

If the detector would be sensitive to the empty state, i.e.,

$$\hat{H}_{\text{measure}} = \hat{a}_d \hat{a}_d^\dagger \left(i\zeta \hat{b}^\dagger + \text{h.c.} \right) \quad (19)$$

instead of (12) in the main text, we would get in the interaction picture

$$\begin{aligned} \hat{a}_d(t) &= e^{-i\epsilon_d t} \exp \left\{ -(\zeta \hat{b}^\dagger - \text{h.c.})t \right\} \hat{a}_d(0), \\ \hat{b}(t) &= \hat{b}(0) + \zeta t \hat{a}_d(0) \hat{a}_d^\dagger(0). \end{aligned} \quad (20)$$

Since in the first line, we have only a flip in sign of ζ in comparison to (13) in the main text, the arguments raised there for the dot occupation prevail in this case and we retain (14) in the main text (assuming of course the same initial conditions).

This is different however for the detector occupation. In this case, due to $\text{Tr} \left\{ \hat{b}^\dagger(t) \hat{b}(t) \hat{\rho}_0 \right\} = \zeta^2 t^2$, a detector signal is seen already for $\gamma_{\mathbf{k}} = 0$ for an initially empty dot. Up to second order, we get

$$\begin{aligned} \langle \hat{b}^\dagger \hat{b} \rangle_t &= \zeta^2 t^2 \\ &+ \zeta^2 \int_0^t dt_1 \int_0^t dt_2 \int_{\text{F}} d^2k |\gamma_{\mathbf{k}}|^2 \exp \left\{ -\frac{\zeta^2}{2} (t_1 - t_2)^2 \right\} \\ &\times [t_1 t_2 + t|t_1 - t_2| - t^2] \exp \{ -i(\epsilon_d - \epsilon_{\mathbf{k}})(t_1 - t_2) \}, \end{aligned} \quad (21)$$

where the temporal crossover of the second order contribution is much harder to observe as the first order contribution is dominant. Thus, to see Zeno signatures in such a detector it would be more suitable to consider the reverse process of an electron tunnelling out of the dot.

Zeno effect and reservoir characteristics

To investigate how the simple two-level picture is influenced by a continuous reservoir, one may instead consider

a finite-chain Hamiltonian (terms with a finite homogeneous on-site energy may be easily added)

$$\hat{H}_N^{1d} = \gamma \sum_{n=1}^{N-1} [|n\rangle \langle n+1| + \text{h.c.}] , \quad (22)$$

where γ denotes the tunnelling rate and $N = 2$ recovers the example in the introduction of the main text. Since the model is homogeneous, an explicit diagonalization is possible via the transformation

$$|n\rangle = \sqrt{\frac{2}{N+1}} \sum_{k=1}^N \sin\left(\frac{\pi kn}{N+1}\right) |E_k\rangle , \quad (23)$$

and in terms of the new basis $|E_k\rangle$ the Hamiltonian becomes diagonal

$$\hat{H}_N^{1d} = \sum_{k=1}^N E_k |E_k\rangle \langle E_k| , \quad E_k = -2\gamma \cos\left(\frac{\pi k}{N+1}\right) \quad (24)$$

This facilitates the computation of the propagator and derived time-dependent quantities. For example, the probability of an initial excitation to remain at the first site becomes

$$\begin{aligned} P_{\text{stay}}^{N,1d}(t) &= \left| \langle 1| e^{-i\hat{H}_N^{1d}t} |1\rangle \right|^2 \\ &= \left| \sum_{k=1}^N e^{-iE_k t} \frac{2}{N+1} \sin^2\left(\frac{\pi k}{N+1}\right) \right|^2 , \end{aligned} \quad (25)$$

which for $N = 2$ just reduces to the $\cos^2(\gamma t)$ expression. For an infinitely long chain we may represent the sum by an analytically solvable integral to obtain

$$P_{\text{stay}}^{\infty,1d}(t) = \left| \frac{\mathcal{J}_1(2\gamma t)}{\gamma t} \right|^2 . \quad (26)$$

For higher-dimensional homogeneous lattices, the calculations can be linked to the one-dimensional case. For example, in two-dimensions we can write the Hamiltonian as

$$\begin{aligned} \hat{H}_{N_x N_y}^{2d} &= \gamma \sum_{n_x=1}^{N_x-1} \sum_{n_y=1}^{N_y} [|n_x n_y\rangle \langle n_x+1, n_y| + \text{h.c.}] \\ &\quad + \gamma \sum_{n_x=1}^{N_x} \sum_{n_y=1}^{N_y-1} [|n_x n_y\rangle \langle n_x, n_y+1| + \text{h.c.}] \\ &= \hat{H}_{N_x}^{1d} \otimes \mathbf{1}_{N_y} + \mathbf{1}_{N_x} \otimes \hat{H}_{N_y}^{1d} . \end{aligned} \quad (27)$$

The trivial tensor product decomposition of the Hamiltonian then yields in D dimensions

$$P_{\text{stay}}^{\infty,Dd}(t) = \left| \frac{\mathcal{J}_1(2\gamma t)}{\gamma t} \right|^{2D} . \quad (28)$$

However, one-dimensional chain representations remain also useful for generic reservoirs. For example,

starting from a representation where the reservoir (described by sites $2 \dots N$) is diagonal, the Hamiltonian reads

$$\begin{aligned} \hat{H} &= \epsilon |1\rangle \langle 1| + \sum_{k=2}^N \epsilon_k |k\rangle \langle k| \\ &\quad + \sum_{k=2}^N [t_k |1\rangle \langle k| + t_k^* |k\rangle \langle 1|] , \end{aligned} \quad (29)$$

where ϵ is the system energy, ϵ_k are the reservoir energies, and t_k describe the system-reservoir tunnelling amplitudes. We can always introduce a new basis in the reservoir only

$$|k\rangle = \sum_{q=2}^N u_{kq} |\bar{q}\rangle , \quad (30)$$

where (u_{kq}) is a unitary matrix with $u_{11} = 1$ and $u_{1,k \geq 2} = u_{k \geq 2,1} = 0$. To further specify the transformation, we additionally impose the conditions

$$\begin{aligned} \delta_{q2} &= \sum_{k=2}^N \frac{t_k^*}{\sqrt{\sum_{\ell=2}^N |t_\ell|^2}} u_{kq} & : & \quad q \geq 2 , \\ \Omega_q \delta_{qq'} &= \sum_{k=2}^N \epsilon_k u_{kq} u_{kq'}^* & : & \quad q, q' \geq 3 . \end{aligned} \quad (31)$$

These conditions can be fulfilled by interpreting the u_{kq} coefficients as eigenvector entries for an $(N-1) \times (N-1)$ hermitian diagonalization problem

$$\begin{aligned} M &= (\mathbf{1} - \mathbf{v}\mathbf{v}^\dagger) \begin{pmatrix} \epsilon_2 & 0 & \dots & 0 \\ 0 & \ddots & \ddots & \vdots \\ \vdots & \ddots & \ddots & 0 \\ 0 & \dots & 0 & \epsilon_N \end{pmatrix} (\mathbf{1} - \mathbf{v}\mathbf{v}^\dagger) , \\ \mathbf{v} &= \frac{1}{\sqrt{\sum_{\ell=2}^N |t_\ell|^2}} \begin{pmatrix} t_2 \\ \vdots \\ t_N \end{pmatrix} . \end{aligned} \quad (32)$$

With conditions (31), the Hamiltonian is recast into

$$\begin{aligned} \hat{H} &= \epsilon |1\rangle \langle 1| + \gamma_{\text{RC}} [|1\rangle \langle \bar{2}| + |\bar{2}\rangle \langle 1|] + \Omega_{\text{RC}} |\bar{2}\rangle \langle \bar{2}| \\ &\quad + \sum_{k=3}^N [\tau_k |\bar{2}\rangle \langle \bar{k}| + \tau_k^* |\bar{k}\rangle \langle \bar{2}|] + \sum_{k=3}^N \Omega_k |\bar{k}\rangle \langle \bar{k}| , \\ \gamma_{\text{RC}} &= \sqrt{\sum_{\ell=2}^N |t_\ell|^2} , \quad \Omega_{\text{RC}} = \sum_{k=2}^N \epsilon_k |u_{k2}|^2 = \sum_{k=2}^N \epsilon_k \frac{|t_k|^2}{\gamma_{\text{RC}}^2} , \\ \tau_k &= \sum_{q=2}^N \epsilon_q u_{q2} u_{qk}^* = \sum_{q=2}^N \epsilon_q \frac{t_q}{\gamma_{\text{RC}}} u_{qk}^* . \end{aligned} \quad (33)$$

In contrast to the starting Hamiltonian (29), the original system $|1\rangle$ is now first coupled to a collective coordinate

$|\bar{2}\rangle$ with energy Ω_{RC} via the amplitude γ_{RC} . The collective coordinate $|\bar{2}\rangle$ is then in turn coupled to the residual reservoir just as in the original Hamiltonian the mode $|1\rangle$ was coupled to its reservoir. Thus, since this Hamiltonian is structurally equivalent to our initial one, one can apply the procedure recursively. Eventually, this will map the reservoir to a (non-homogeneous) chain.

To consider reservoirs of infinite size we introduce the original spectral coupling density $\Gamma(\omega) \equiv 2\pi \sum_k |t_k|^2 \delta(\omega - \epsilon_k)$ as a continuous (not necessarily differentiable) function. The tunnelling amplitude and energy of the collective coordinate maintain their meaning and can be written as

$$\gamma_{\text{RC}}^2 = \frac{1}{2\pi} \int \Gamma(\omega) d\omega, \quad \Omega_{\text{RC}} = \frac{1}{2\pi\gamma_{\text{RC}}} \int \omega \Gamma(\omega) d\omega \quad (34)$$

The residual (new) spectral coupling density $\bar{\Gamma}(\omega) \equiv 2\pi \sum_k |\tau_k|^2 \delta(\omega - \Omega_k)$ is also a function of the old spectral coupling density

$$\bar{\Gamma}(\omega) = \frac{4\gamma_{\text{RC}}^2 \Gamma(\omega)}{\left[\frac{1}{\pi} \mathcal{P} \int \frac{\Gamma(\omega')}{\omega' - \omega} d\omega' \right]^2 + [\Gamma(\omega)]^2}. \quad (35)$$

This formula is more complicated to obtain but can for example be found by solving the Heisenberg equations of motion for $|1\rangle \langle 1|$ according to Eq. (29) and Eq. (33) in analogy to Ref. [50]. Shortcutting this, one may also express the old spectral coupling density by

$$\begin{aligned} \Gamma(\omega) &= \int \langle 1| e^{+i\hat{H}_B\tau} \hat{H}_I e^{-i\hat{H}_B\tau} \hat{H}_I |1\rangle e^{+i\omega\tau} d\tau \\ &= \gamma_{\text{RC}}^2 \int \langle \bar{2}| e^{-i\hat{H}_B\tau} |\bar{2}\rangle e^{+i\omega\tau} d\tau, \end{aligned} \quad (36)$$

where $\hat{H}_I = \hat{h} + \hat{h}^\dagger$ with $\hat{h} = \sum_k t_k |1\rangle \langle k| = \gamma_{\text{RC}} |1\rangle \langle \bar{2}|$ and $\hat{H}_B = \sum_k \epsilon_k |k\rangle \langle k| = \Omega_{\text{RC}} |\bar{2}\rangle \langle \bar{2}| + \sum_k [\tau_k |\bar{2}\rangle \langle \bar{k}| + \tau_k^* |\bar{k}\rangle \langle \bar{2}|] + \sum_k \Omega_k |\bar{k}\rangle \langle \bar{k}|$. Inserting the operators in the original basis recovers the definition of the old spectral coupling density, whereas inserting the new basis yields an expression for the residual (new) spectral coupling density. Defining $P_{22}(\tau) = \langle \bar{2}| e^{-i\hat{H}_B\tau} |\bar{2}\rangle$, one obtains for its Laplace transform $p_{22}(z) = \int P_{22}(\tau) e^{-z\tau} d\tau$ the expression

$$p_{22}(z) = \frac{1}{z + i\Omega_{\text{RC}} + \frac{1}{2\pi} \int \frac{\bar{\Gamma}(\omega')}{z + i\omega'} d\omega'}. \quad (37)$$

For a function obeying $f(t) = f^*(-t)$, its Laplace transform $F(z) = \int_0^\infty f(t) e^{-zt} dt$ provides information about its even and odd Fourier transforms

$$\begin{aligned} \lim_{\epsilon \rightarrow 0^+} 2 \operatorname{Re} F(\epsilon - i\omega) &= \int f(t) e^{+i\omega t} dt = \tilde{f}(\omega), \\ \lim_{\epsilon \rightarrow 0^+} 2i \operatorname{Im} F(\epsilon - i\omega) &= \int f(t) \operatorname{sgn}(t) e^{+i\omega t} dt \\ &= \frac{i}{\pi} \mathcal{P} \int \frac{\tilde{f}(\omega')}{\omega - \omega'} d\omega'. \end{aligned} \quad (38)$$

From the first line above, it follows that $\Gamma(\omega) = \gamma_{\text{RC}}^2 \lim_{\epsilon \rightarrow 0} [p_{22}(\epsilon - i\omega) + \text{h.c.}]$, and we obtain a relation between the old and the residual (new) spectral coupling densities

$$\Gamma(\omega) = \frac{\gamma_{\text{RC}}^2 \bar{\Gamma}(\omega)}{\left[\omega - \Omega_{\text{RC}} - \mathcal{P} \int \frac{\bar{\Gamma}(\omega')}{\omega - \omega'} \frac{d\omega'}{2\pi} \right]^2 + \left[\frac{\bar{\Gamma}(\omega)}{2} \right]^2}, \quad (39)$$

which precisely corresponds to the inverse reaction-coordinate mapping, cf. Eq. (12) in Ref. [51]. Considering the imaginary part of the Laplace transform instead allows – together with the relation above – to solve also for the residual spectral coupling density $\bar{\Gamma}(\omega)$ in dependence of the old one, yielding precisely Eq. (35), which corresponds to the particle mapping for bosons or fermions, cf. Eqns. (11) and (14) of Ref. [50].

To relate this to the Zeno time, we note that for a single resonant level model, the Zeno transition time is directly given by the spectral coupling density

$$T_* = \frac{2\pi\Gamma(\epsilon)f(\epsilon)}{\int \Gamma(\omega)f(\omega)d\omega} \rightarrow \frac{2\pi\Gamma(\epsilon)}{\int \Gamma(\omega)d\omega}, \quad (40)$$

where $f(\omega) \equiv [e^{\beta(\omega - \mu)} + 1]^{-1}$ denotes the Fermi function with inverse temperature β and chemical potential μ and the limit holds for a completely filled reservoir (high chemical potentials and low temperatures).

If we consider a Lorentzian spectral coupling density

$$\Gamma(\omega) = \frac{\Gamma\delta^2}{(\omega - \epsilon_B)^2 + \delta^2}, \quad (41)$$

this would imply $\bar{\Gamma}(\omega) = 2\delta$ and for the Zeno time $T_* = \frac{2\delta}{(\epsilon - \epsilon_B)^2 + \delta^2}$, which can be made very large when $\epsilon \approx \epsilon_B$ and $\delta \rightarrow 0$. Indeed, considering the limit $\delta \rightarrow 0$ and $\Gamma \rightarrow \infty$ such that $\Gamma\delta$ remains constant, we obtain an effective two-level system

$$\hat{H}_S = \epsilon |1\rangle \langle 1| + \epsilon_B |\bar{2}\rangle \langle \bar{2}| + \sqrt{\frac{\Gamma\delta}{2}} (|1\rangle \langle \bar{2}| + \text{H.c.}) \quad (42)$$

that is decoupled from the residual reservoir.

Thus, generic reservoirs may reproduce the two-level picture when they support a highly peaked spectral coupling density.

Zeno and Anti-Zeno dynamics

So far, we discussed the standard Zeno effect, i.e., how frequent measurements slow down the quantum evolution compared to the unperturbed one. Depending on the level configurations, one may however also observe an acceleration of the decay dynamics, termed anti-Zeno [42] or inverse Zeno [8] effect. Generically, one may express the unperturbed expectation value of a positive definite operator \hat{O} with initial expectation value $\langle \hat{O} \rangle_0 = 1$ for a quantum system subject to Hamiltonian

\hat{H} as $P_{\text{stay}}(t) = \text{tr}\{\hat{O}e^{-i\hat{H}t}\rho_0e^{+i\hat{H}t}\} \equiv e^{-R(t)\cdot t}$. The effective rate $R(t)$ is in general different from its Fermi Golden Rule value $R_{\text{FG}} = \text{const.}$ If projective measurements are performed at time intervals τ , the remainder probability after n measurements with $t = n\tau$ will be given by $[e^{-R(\tau)\tau}]^n = e^{-R(\tau)t}$ as compared to a measurement-free (Fermi Golden Rule) evolution $e^{-R_{\text{FG}}t}$ for large times t . Thus, when $R(\tau) > R_{\text{FG}}$ one may actually accelerate the decay of the initial state by measurement (anti-Zeno effect), whereas when $R(\tau) < R_{\text{FG}}$ the decay may be slowed down (conventional Zeno effect). The relevant effective decay rate can be obtained via

$$R(\tau) = \frac{-\ln P_{\text{stay}}(\tau)}{\tau}. \quad (43)$$

This is already observable for the previously discussed reservoir with a Lorentzian spectral coupling density. To connect with the main text, we discuss this for the single resonant level subject to a reservoir with the Gaussian model below.

Example: Single resonant level with exponential spectral function

The single resonant level coupled to a reservoir is described by the fermionic total Hamiltonian

$$\hat{H} = \epsilon_d \hat{n}_d + \sum_k \epsilon_k \hat{c}_k^\dagger \hat{c}_k + \sum_k \left[t_k \hat{d}^\dagger \hat{c}_k + t_k^* \hat{c}_k^\dagger \hat{d} \right], \quad (44)$$

where the first term denotes the dot Hamiltonian with $\hat{n}_d = \hat{d}^\dagger \hat{d}$ and on-site energy ϵ_d , the second term the reservoir with energies ϵ_k , and the last term the interaction, for continuum reservoirs described by the spectral coupling density $\Gamma(\omega) = 2\pi \sum_k |t_k|^2 \delta(\omega - \epsilon_k)$. When we consider the Gaussian model (3) from the main text, the spectral coupling density in absence of a magnetic field assumes an exponentially decaying form

$$\Gamma(\omega) = \Gamma_0 e^{-\lambda\omega} \Theta(\omega), \quad (45)$$

where $\Gamma_0 = m\gamma_0^2$ and $\lambda = 2m\ell^2$. Thus, for small dot size ℓ , the spectral coupling density decays very slowly and can be considered nearly flat. The Zeno transition time from the main text becomes $T_* = 2\pi\lambda e^{-\lambda\epsilon_d} \Theta(\epsilon_d)$. In contrast, when we turn on the magnetic field, the levels in the reservoir immediately obtain a finite splitting (Landau levels), which increases linearly with the field strength.

We can address the dot occupation dynamics with several methods, which we make explicit for an initially empty dot $\langle \hat{d}^\dagger \hat{d} \rangle_0 = 0$ and a thermally occupied reservoir $\langle \hat{c}_k^\dagger \hat{c}_k \rangle_0 = f(\epsilon_k)$ with Fermi function $f(\omega) = [e^{\beta(\omega-\mu)} + 1]^{-1}$:

First, the system dynamics can be solved exactly by solving the Heisenberg equations of motion [52] for the

fermionic operators \hat{d} and \hat{c}_k . After some algebra this yields for the dot occupation

$$\langle \hat{n}_d \rangle_t^{\text{ex}} = \frac{1}{2\pi} \int \Gamma(\omega) f(\omega) |g(\omega, t)|^2 d\omega, \quad (46)$$

$$\int_0^\infty g(\omega, t) e^{-st} dt = \frac{1}{(s + i\omega) \left(s + i\epsilon_d + \frac{1}{2\pi} \int \frac{\Gamma(\omega')}{s + i\omega'} d\omega' \right)},$$

which is still hard to evaluate due to the required inversion of a Laplace transform. At low temperatures, the Fermi function becomes a step function $f(\omega) \rightarrow \Theta(\mu - \omega)$.

Second, we can use the second-order perturbative solution analogous to the discussion in the main text

$$\langle \hat{n}_d \rangle_t^{\text{so}} = \frac{t^2}{2\pi} \int \Gamma(\omega) f(\omega) \text{sinc}^2 \left[(\omega - \epsilon_d) \frac{t}{2} \right] d\omega, \quad (47)$$

which is already much simpler to evaluate. The above formula has the short-term regimes $\langle \hat{n}_d \rangle_t \approx \frac{t^2}{2\pi} \int \Gamma(\omega) f(\omega) d\omega$ and Fermi Golden Rule regimes $\langle \hat{n}_d \rangle_t \approx t\Gamma(\epsilon_d) f(\epsilon_d)$. In regimes where the perturbative treatment is valid (i.e., where $\langle \hat{n}_d \rangle_t$ is small, the effective decay rate (43) can be further simplified

$$R(t) = \frac{-\ln[1 - \langle \hat{n}_d \rangle_t]}{t} \approx \frac{\langle \hat{n}_d \rangle_t^{\text{so}}}{t} = \int \Gamma(\omega) f(\omega) \frac{t}{2\pi} \text{sinc}^2 \left[(\omega - \epsilon_d) \frac{t}{2} \right] d\omega, \quad (48)$$

which generically vanishes at small times (Zeno regime) and assumes the Fermi Golden rule rate $R_{\text{FG}} = \Gamma(\epsilon_d) f(\epsilon_d)$ at large times.

Third, we can perform the mapping to an effective two-level system (34) coupled to a residual reservoir with modified spectral coupling density (35) (also called spectral function). If the latter is small, we can (for the initial times we are interested in) neglect the residual spectral coupling density and consider only the effective two-level dynamics

$$\langle \hat{n}_d \rangle_t^{2\text{L}} = \frac{4\gamma_{\text{RC}}^2 \sin^2 \left[\frac{t}{2} \sqrt{4\gamma_{\text{RC}}^2 + (\epsilon_d - \Omega_{\text{RC}})^2} \right]}{4\gamma_{\text{RC}}^2 + (\epsilon_d - \Omega_{\text{RC}})^2}. \quad (49)$$

For the spectral coupling density (45), the mapping relation (34) yield for the effective two-level system the explicit parameters

$$\gamma_{\text{RC}} = \sqrt{\frac{\Gamma_0}{2\pi\lambda}}, \quad \Omega_{\text{RC}} = \frac{1}{\lambda}, \quad (50)$$

whereas the residual spectral coupling density must be computed numerically via (35).

The results are depicted in Fig. 2.

The first row displays the situation of a dot level inside the reservoir spectral window, which however has a quickly decaying spectral coupling density (top right sketch), such that the effective two-level picture (dashed green curves) applies well. For this off-resonant case, one

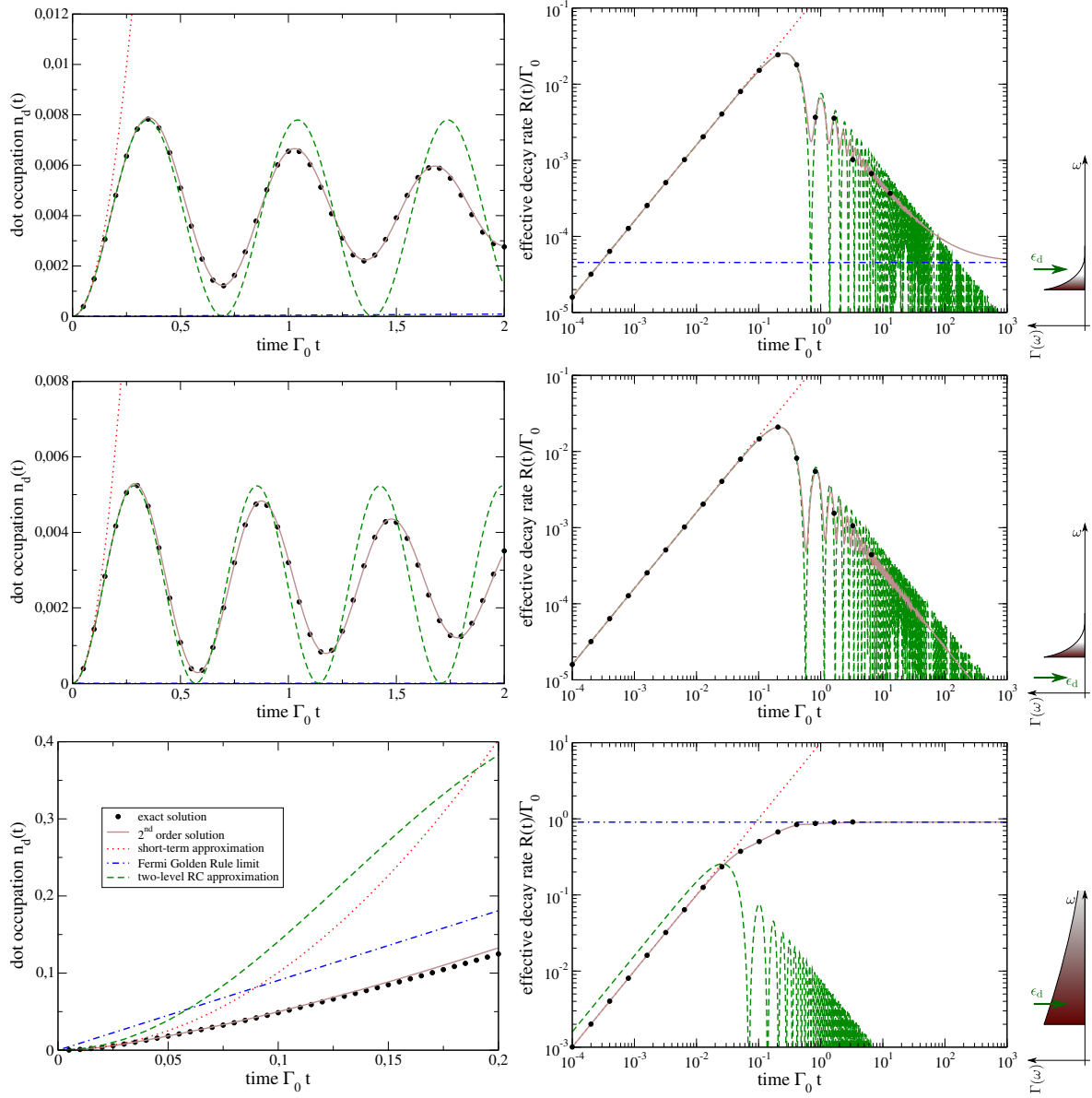


FIG. 2. Dot occupation vs. time (left column) and effective decay rate (middle column) for a dot weakly coupled ($\Gamma_0 = 0.1|\epsilon_d|$) to a low-temperature and high-potential ($\beta|\epsilon_d| = 100$ and $\mu = 10|\epsilon_d|$) reservoir described by spectral coupling density (45) for different configurations (sketched in the right column). In the top row, the level is inside the reservoir window with $\epsilon_d > 0$ and quickly decaying spectral coupling density $\lambda = 10/\epsilon_d$, in the middle row, the level is below the reservoir window with $\epsilon_d < 0$ and quickly decaying spectral coupling density $\lambda = 10/|\epsilon_d|$, and in the bottom row, the level inside the reservoir window with $\epsilon_d > 0$ and slowly decaying spectral coupling density $\lambda = 0.1/\epsilon_d$. Black symbols denote the exact solution (46) and the full effective rate $-t^{-1} \ln(1 - \langle n_d \rangle_t^{\text{ex}})$, respectively, solid brown curves the second order solution (47) and the approximate effective decay rate (48), respectively. Dotted red and dash-dotted blue curves denote the short-term and Fermi Golden Rule approximations to the second order perturbative solution, respectively. Finally, the dashed green curves depict the evolution due to the isolated effective two-level system (49) with parameters chosen according to (50) and the corresponding approximate effective decay rate (48), respectively.

finds a transition from a Zeno-regime to an anti-Zeno regime (where the effective decay rate is larger than the Fermi Golden Rule value, top right plot) before the Fermi Golden Rule regime is reached for long times. Thus, the discussion from the main text is not applicable for this special case. However, since the two-level picture applies

to this regime, we can estimate the time range within which anti-Zeno effects are observable by equating the rates according to the two-level picture with the Fermi Golden Rule result $\langle n_d \rangle_t^{2L}/t^* = \Gamma(\epsilon_d)f(\epsilon_d)$.

In the second row, the dot level is outside the reservoir spectral window, such that the Fermi Golden Rule result

would forbid the dot to be loaded (middle left plot), and the corresponding rate just vanishes (middle right plot). Nevertheless, loading is possible at finite times beyond leading order. Projective measurements would manifest these virtual processes, such that there is no Zeno regime but only an anti-Zeno regime in this case. Another way to look at this behaviour is that for small times, the energy-time uncertainty relation does not allow to resolve the energy mismatch between system and reservoir.

The bottom row depicts the situation discussed in the main text, where the spectral coupling density of the reservoir decays slowly. Although the effective two-level picture does not apply well (the residual spectral coupling density (35) is not negligible), the maximum height of the oscillations demonstrates that an anti-Zeno effect is out of reach for this scenario. One finds a direct transition between Zeno and Fermi Golden Rule regimes, and the Zeno time T^* is a useful diagnostic measure.